2014 International Conference on Unmanned Aircraft Systems (ICUAS)
May 27-30, 2014. Orlando, FL, USA

Tethered vs. Free Flight Force Determination of the DelFly II Flapping Wing Micro Air Vehicle

J.V.Caetano*†, M. Percin‡, C.C. de Visser*, B. van Oudheusden‡, G.C.H.E de Croon*, C. de Wagter*, B. Remes* and M. Mulder*
*Section of Control and Simulation, Faculty of Aerospace Engineering, Delft University of Technology, Delft, The Netherlands
†Air Force Research Laboratory, Portuguese Air Force Academy, Sintra, Portugal
‡Section of Aerodynamics, Faculty of Aerospace Engineering, Delft University of Technology, Delft, The Netherlands
Corresponding author: j.v.caetano@tudelft.nl; DelFly research contact: microuav@gmail.com

Abstract*—The determination of dynamic forces acting on a Flapping Wing Micro Aerial Vehicle (FWMAV) is a challenging task due to the unsteady nature of force generation mechanisms. To assure a proper force identification in future researches, this work compares two different methods to obtain the longitudinal forces acting on FWMAVs and discusses their applicability regions. The methods were 1) calculation of forces from the recordings of the FWMAV's position in a free flight condition; 2) direct force measurements in a tethered flight condition in a wind tunnel. The DelFly II is used as the FWMAV test platform in the measurements. During free flight experiments, its position and attitude were recorded at a rate of 200Hz using an external visual tracking system, whose acquired information was then analyzed to obtain the flight states and calculate the forces and moments that act on the platform during flight, under a set of kinematic assumptions. Subsequently, similar flight conditions were tested in the tethered situation. An ATI Nano-17 Titanium force transducer was used to measure time-resolved forces. The results for the most common flight regime of the DelFly, which is a slow forward flight at a high body pitch angle, are presented. It is shown that the tethered force balance tests agree with the free flight data when assessing the aerodynamic forces that are perpendicular to the stroke plane of the flapping wing. However, the forces that act along the stroke plane are coupled with structural dynamic terms, thus affecting the final lift and thrust identification. These results point to inadequate force identification in fixed point force measurements, due to effect the of the dynamic modes of the FWMAV body, thus advising proper cross-comparing between experimental methods.

I. Introduction

The growing number of studies that is dedicated to understand flapping wing flight and control envisions the development of fast and maneuverable micro scale flapping wing aerial vehicles with many advantages over fixed and rotary wing platforms, e.g, the extended flight envelope, agility, efficiency and adaptability to a specific mission.

In this field, the research can be divided into two main approaches: bottom-up and top-down. Bottom-up strategies primarily focus on the fundamental understanding of flapping wing flight, by using either experimental investigations with full kinematic models of flapping mechanisms or fundamental approaches to explain the fluids' behavior and interactions around flapping wings. These types of models are also used to build complete dynamics simulations with connected control laws. The seminal works done by Ellington [1]–[3], Dickinson [4] and Wang [5], [6] have greatly contributed to the understanding of the aerodynamic mechanisms of insect flight. Gogulapati and Friedmann [7], Aono et al. [8], Kang et al. [9] have deepened the knowledge in fluid-structure interactions in flapping flight. In parallel, other important work from Ansari et al. [10], [11], Bolender [12], Orlowsky et al. [13], [14] focused on flight kinematics and contributed to the creation of extended wing beat and full body flight kinematic and dynamic models.

Top-down approaches, on the other hand, are characterized by the construction of phenomenological models that can describe the behavior of Flapping Wing Micro Aerial Vehicles (FWMAVs) in free flight. Important contributors have been Sibilski [15], [16], Dietl and Gracia [17], [18], Wood et al. [19], [20], Fearing et al. [21], [22], Grauer [23], [24] and Lee and Han [25]. These studies focus on the development or use of man-made FWMAVs using a general comprehension of the fundamental models, that are test-flown and iterated with the final goal of having a controllable highly maneuverable platform whose behavior and dynamics can be predicted and controlled. The phenomenological models can be based on empirical or more fundamental formulations and are generally devised from experimental testing using system identification techniques.

Both bottom-up and top-down approaches share a common ground: the experimental testing and procedures. These are generally measurements of forces and flow characteristics in a wind or water tunnel by satisfying geometric, kinematic and dynamic similarities or measurements in free flight conditions by use of a proper model of the FWMAV. The aforementioned strategies can provide very important information for the development and validation of aerodynamic and dynamic models. However, as well as complementing each other, the results can sometimes lead to a dichotomy in the conclusions. As an example, wind tunnel testing combined with force balance measurements are good for describing the dominant forces and moments acting on the FWMAV at specific test points. However, these are only static tests that do not capture the FWMAV's dynamical response or stability.

978-1-4799-2376-2/14/$31.00 ©2014 IEEE

Currently, numerous researches have relied on force balance and wind tunnel measurements as the main experimental setup for the characterization and understanding of the lift and thrust generating mechanisms of tailless and tailed FWMAVs, see [26]–[29]. These studies, however, did not consider effects of vibrations and force measuring locations, nor have they cross-compared the corresponding data obtained from the collected information with the free flying ornithopter. Other studies, on the other hand, have focused on extracting the forces that act on free flying FWMAVs, such as [24], [30], without, comparing the results with force balance mechanisms or numerical simulations.

More recently, Caetano et al. [31], [32] reconstructed the forces and moments that acted on a tailed ornithopter (the DelFly II) in a series of more than 200 flight tests that covered the FWMAV's full flight envelope. The tests were performed in a motion cueing flight chamber in which several identification maneuvers were performed with a flying DelFly II. However, these studies did not compare the free flight reconstructed forces with high precision force balance tests, thus not measuring the fidelity of their results.

On the other hand, Lee and Han [25] succeeded in performing wind tunnel tethered force measurements with a moving balance system, that enabled some degree of freedom in the flapping motion and compared the results with those obtained by free flying the ornithopter in a visual tracking system. Nevertheless, this study aimed at determining only the flap average generated forces, resulting in a crude force comparison between the methods.

There is the need for assessing the fidelity of both free flight and tethered wind tunnel force measurement techniques, that are tendentiously assumed to be correct and accurate. Hence, the presented study aims at bridging the knowledge gap of sub-flap Lift and Trust generation mechanisms, by comparing tethered wind tunnel force balance measurements with free flight force calculation at the same trim points. Furthermore, it alerts for the main errors of considering separate test methodologies for flapping wing force characterization and produces recommendations for proper force measurements. Figure 1 presents the general approach and this article's current contribution. The DelFly II FWMAV is introduced in Section II, followed by the experimental setup description. Section III compares the results obtained on both experimental procedures and discusses the differences. The article ends with the main conclusions and recommendations in Section IV.

II. Experimental Setup Overview

This section describes the DelFly II FWMAV model, the test setups, data processing techniques and assumptions made for the calculation of the forces that act on the FWMAV.

A. DelFly II Micro Aerial Vehicle

The DelFly II is a FWMAV with four wings that flap with the same stroke plane, by means of one single motor. It is configured with an inverted 'T' tail and is capable of carrying different payloads, e.g., a simple radio control (RC) receiver or a programmable autopilot and stereo-vision cameras with live telemetry and on-screen display. Its inherent static stability and large flight envelope (with velocity ranging from hover to 8m/s) make it a very suitable platform higher level implementations like automatic control and bio-inspired aerodynamic system identification.

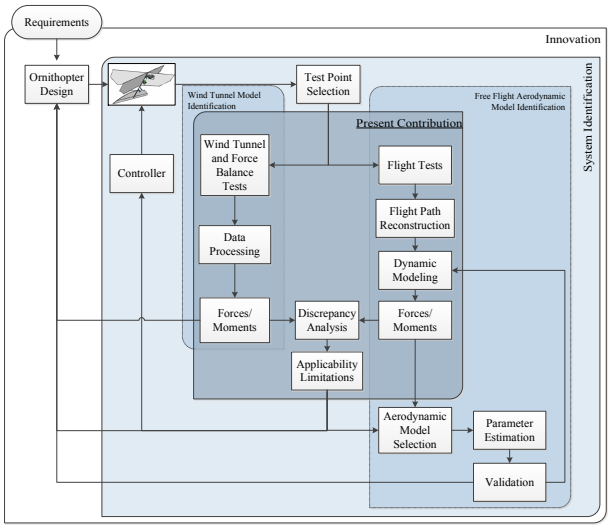

Fig. 1. Current contribution flowchart with associated framework.

The DelFly II (henceforth named as the DelFly) that was used in the current test campaign weighs 17.4 grams with full payload. Its Center of Gravity (CG) is located at 72 mm from the wing leading edge in the direction parallel to the carbon rod body along negative body axis direction ($-\overrightarrow{X_b}$, Figure 3) and 5 mm bellow that rod, in the $-\overrightarrow{Z_b}$ direction.

B. Free Flight Tests

The procedure started with a series of flight tests at specified trim conditions [32], [33]. Afterwards, Flight Path Reconstruction techniques were applied that, together with a set of assumptions (Section II-B3), led to the proposed dynamics model and consequent calculation of the acting forces and moments.

1) Experimental Setup: A motion capturing facility[1] was used to track the DelFly's position at 200Hz, using 8 markers that were placed on its fixed structure and control surfaces[2], as shown in Figure 2.

The FWMAV was configured to fly at specific trim conditions, that were enforced by adjusting its CG, the flapping frequency and the elevator and rudder inputs. A total of 107 flight tests were carried out at different CG positions, velocities and trim conditions, covering the ornithopter's flight envelope. A better visualization of the experimental setup and flight tests can be found in the video on [34].

[1]the US Air Force Research Laboratory's Micro Air Vehicles Integration and Application Institute (μAVIARI) flight chamber

[2]more information about the flight chamber and marker placement can be found in Caetano et al. [33]

Fig. 2. Markers' positions on the DelFly, respectively placed at the nose, trailing edge of the wing, wing stiffeners' intersection with leading edge rod, fixed horizontal and vertical stabilizers, elevator and rudder.

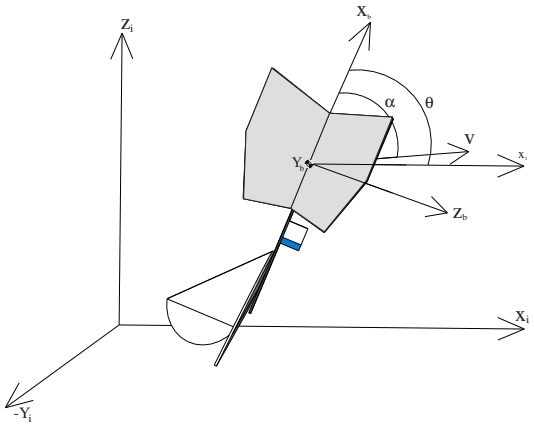

Fig. 3. Inertial $(\overrightarrow{X_i}, \overrightarrow{Y_i}, \overrightarrow{Z_i})$ and Body $(\overrightarrow{X_b}, \overrightarrow{Y_b}, \overrightarrow{Z_b})$ reference frames. Pitch (θ) is measured as the angle between the $\overrightarrow{X_b}$ and $\overrightarrow{X_i}$ and the angle-of-attack α as the relative wind angle in the X_bZ_b plane, measured from $\overrightarrow{X_b}$.

2) Flight Path Reconstruction: Flight Path Reconstruction techniques were applied to estimate the DelFly's states during the flight tests. The coordinates of the 8 markers were transformed from the flight chamber's (considered as Inertial) reference frame $(\overrightarrow{X_i}, \overrightarrow{Y_i}, \overrightarrow{Z_i})$ to the DelFly's Body reference frame $(\overrightarrow{X_b}, \overrightarrow{Y_b}, \overrightarrow{Z_b})$, as indicated in Figure 3. The unit vectors of the Body frame were used to build the direct cosines matrix, from which the Euler angles were computed by comparing the respective entries of the 3-2-1 rotation matrix [32] described in Eq. 1, where c and s represent cos and sin, respectively.

$$\mathcal{R}_{bi} = \begin{bmatrix} c\theta c\psi & c\theta s\psi & -s\theta \\ c\phi c\theta c\psi - c\phi c\psi & c\phi c\psi + s\phi s\theta s\psi & s\phi c\theta \\ s\phi s\psi + c\phi s\theta c\psi & s\phi c\psi - c\phi s\theta s\psi & c\phi c\theta \end{bmatrix} \quad (1)$$

Different differentiation approaches will produce dissimilar information smoothing and error magnification. For the current case, the velocities and accelerations were obtained by differentiating the position of the FWMAV's CG with respect to time using first and second order three point central difference schemes, respectively - this reduces the noise error amplification by a factor of 2 when compared to two point finite differences, while preventing excessive data averaging and smoothing caused by other approaches, i.e., decreasing the sampling frequency or 5 point differentiation schemes. The angular velocities (p, q, r) were obtained from the Euler angles using Eq. 2.

$$\begin{bmatrix} p \\ q \\ r \end{bmatrix} = \begin{bmatrix} 1 & 0 & -\sin\theta \\ 0 & \sin\phi & \sin\phi\cos\theta \\ 0 & -\sin\phi & \cos\phi\cos\theta \end{bmatrix} \begin{bmatrix} \dot{\phi} \\ \dot{\theta} \\ \dot{\psi} \end{bmatrix} \quad (2)$$

The angle of attack (α) was computed from the angular relation between the velocities (u, v, w) in the Body axes, measured at the CG, as indicated in Figure 3, thus not representing the local flapping wing angles. A total of 17 states were reconstructed: Euler angles (ϕ, θ, ψ); velocity $\overrightarrow{V} = (u, v, w)$; accelerations $\overrightarrow{\dot{V}} = (\dot{u}, \dot{v}, \dot{w})$; angular velocities $\overrightarrow{\omega} = (p, q, r)$; angular accelerations $\overrightarrow{\dot{\omega}} = (\dot{p}, \dot{q}, \dot{r})$ and aerodynamic angles angle of attack (α) and side-slip angle (β).

3) Kinematic Formulation: The forces and moments that acted on the FWMAV in free flight were computed under the assumptions of a) non-flapping/rigid body kinematics; b) constant mass and inertia properties; c) non-moving atmosphere; d) non-rotating flat Earth; e) constant air density and gravity; f) symmetric platform.

The selection of assumptions a) and b) for the FWMAV's dynamics is motivated by the need for a simple, flap-averaged model that could be used as a baseline for simple controllers that can run on-board. Moreover, the DelFly is an inherently stable platform that does not require active sub-flap commands over the flapping period for attitude and maneuver control - similar strategy was applied by Dietl and Garcia [35], [36]. The assumption of non-moving atmosphere neglects the vortices and wake structures generated by the flapping flight [37], assuming the flow as being steady around the platform.

The dynamics equations that were devised to compute the longitudinal forces acting on the FWMAV are presented in Eq. 3 [31], which follows the general aircraft equations of motion, with X and Z being the force along the $\overrightarrow{X_b}$ and $\overrightarrow{Z_b}$ (in Figure 3).

$$\begin{aligned} X &= m(g\sin\theta + qw - rv + \dot{u}) \\ Z &= m(-g\cos\phi\cos\theta - qu + pv + \dot{w}) \end{aligned} \quad (3)$$

C. Wind Tunnel Tests

1) Experimental Setup: Experiments were performed in a low-speed wind tunnel at the Aerodynamics Laboratory of Delft University of Technology. The wind tunnel has an open test segment, with cross-section dimensions of 0.6m×0.6m. The free-stream velocity was measured by use of a hot-wire anemometer and set to match with the DelFly's trimmed free flight velocity experienced in the tests mentioned Section II-B.

The wind tunnel contraction was specially designed for very low turbulence laminar flow at very low speeds. A hot-wire measurement downstream of the test section concluded that the turbulence was always under 5% of the free stream velocity, even at 20cm from the nozzle.

Six components of statically measured forces and moments were captured by use of an ATI Nano-17 Titanium force transducer that was attached to a variable pitch mechanism (Figure 4). The sensor is calibrated to have a resolution of 0.149 gram-force without filtering in all directions. The balance mechanism allows the adjustment of the pitch angle of the FWMAV from $-15\,^{\circ}$ to $95\,^{\circ}$. The DelFly pitch angle and wind tunnel free stream were set to different values close to the ones observed in free flight regime.

A microcontroller system was used to regulate the flapping frequency. It logs the electrical commutations of the brushless motor for high resolution rotational information and reads a Hall sensor signal from the wing driving gear for referencing. This information is used with an integrative controller to adjust the power supplied and keep the flapping frequency constant [34].

An in-house programmed Field-Programmable Gate Array (FPGA) system of National Instruments was used for data acquisition the forces and moments, rotational information, as well as motor voltage and current at 12.5kHz.

The relation between the rotational information captured by the microcontroller system and the phase angle of the wings is assessed by means of high speed image capture syncing. A Photron Fastcam SA 1.1 camera was placed in front of the experimental model to record the spatial positions of the leading edges of both upper and lower wings to determine the stroke angle during the flapping cycle. A series of 1200 images were recorded during each test with a recording rate of 1200Hz.

The forces were captured for different conditions corresponding to real ornithopter leveled flight, with the pitch $\theta \in [30; 83]^{\circ}$ and velocity $|\overrightarrow{V}| \in [0.3; 2]$m/s.

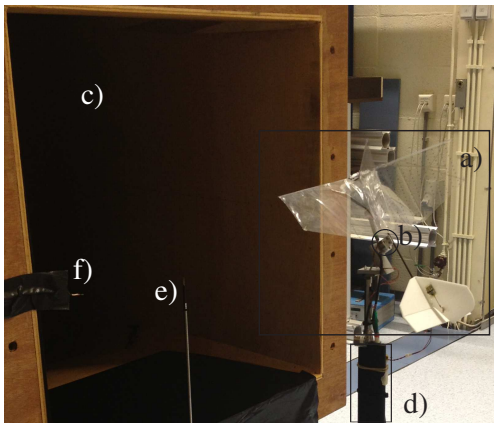

Fig. 4. Wind tunnel experimental setup: a) DelFly FWMAV; b) ATI Nano-17 force transducer; c) open section wind tunnel; d) actuated strut that allows for attitude changes in pitch and yaw; e) hot-wire anemometer; f) thermocouple for temperature corrections.

2) Processing Methods: The high-speed recorded images were pre-processed to improve contrast and to provide a clear image of the leading edges, using built-in functions of MATLAB. Then a Hough transform [38] was performed on the pre-processed images in order to detect the leading edges and to calculate the stroke angles.

The raw force and moment data were filtered by a Chebyshev Type II low-pass filter with -80dB attenuation of the stopband in MATLAB. A forward-backward filtering technique was implemented by use of 'filtfilt' function of MATLAB in order to prevent time-shift of the data. The cut-off frequency is selected as 40 Hz to match the number of harmonics in the free flight estimated forces for the sake of clear comparison.

To further compare the forces measured by the force transducer with the ones calculated from Eq. 3 a virtual displacement was computed using the tethered measured forces and compared with the real displacement in free flight. For this, the DelFly was considered as a point mass and the equations of motion were simplified to $\overrightarrow{F} = m\overrightarrow{a}$. The displacements in vertical direction of the inertial reference frame were then calculated by integrating the acceleration data twice over time by use of a trapezoidal numerical integration method in MATLAB.

III. Results and Discussion

This section presents and discusses the results of the processing methods described before.

Figure 5 presents the distribution of the ornithopter's angle of attack with velocity in the form of a scatter plot. These points correspond to 107 test flights performed with the same FWMAV, in a total recording time of 22 minutes.

Both the free flight and the wind tunnel measurements were analyzed for a recording time of about 10 seconds to capture sufficient number of flapping periods. Despite the FWMAV's oscillation around the trimmed flight condition (variation of flight speed and altitude) and the limited precision of the external tracking system in the free flight measurements, the results were fairly repeatable throughout numerous flapping cycles and different flight regimes. For the sake of clear comparison of the forces within the flap cycle, the results are presented for two flapping cycles for a test point that represents the ornithopter's usual flight condition (Figure 5) for levelled flight, with $\theta = 73°$, $|\overrightarrow{V}| = 0.5$m/s and flapping frequency of 12.5Hz. The pitch angle in the wind tunnel experiments was selected to be close to the average angle of attack experienced in free flight, as indicated in Figure 6(d) - in this case $\theta_{wt} = 78°$.

Both the X and Z forces that were calculated from Eq. 3, using the free flight states, and the X and Z forces that were measured directly from the force transducer in the wind tunnel experiments are presented in Figure 6(a) and (b), shown in blue and red respectively, with dashed lines indicating the cycle-averaged values. The comparison of forces is complemented with the vertical displacement of the FWMAV measured in free flight condition and the predicted motion of a point mass exposed to the forces measured in

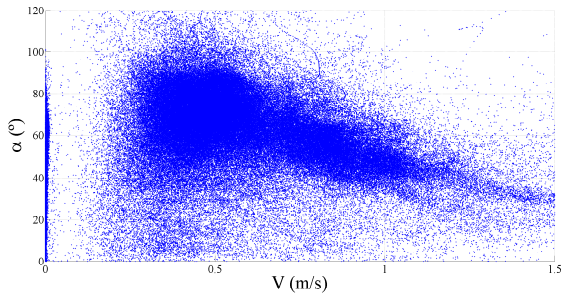

Fig. 5. The DelFly's computed angle-of-attack (α) versus total velocity $|\vec{V}|$. The blue markers correspond to the states recorded each time-step in a total of 107 system identification tests, with a total recording time of approximately 22 minutes. The selected point corresponds to the usual flight regime of the FWMAV $\theta = 73°$, $|\vec{V}| = 0.5m/s$ and flapping frequency of 12.5Hz.

the tethered condition; the comparison of pitch angle; and the variation of upper wing's stroke angle in free flight and tethered conditions, respectively for Figure 6(c), (d) and (e). In all plots, the horizontal axis represents the dimensionless time ($t^* = \delta_t/T_f$, with δ_t and T_f being the elapsed time and flap period, respectively) for two flapping cycles and all quantities were measured at the ornithopter's CG for the free flight case [33].

Differences in the upper wing stroke angle presented in Figure 6(e) can be attributed to the use of different reference points for the calculation of the stroke angle. In the free flight case, reflective markers placed on the wing surface just behind the leading edge (Figure 2) were used for the determination of the stroke angle; whereas, the leading edge spars [39] are used for stroke angle determination in the case of balance measurements. The angle is very similar when the wings at each side of the of the ornithopter are close to each other in a closed position (i.e., clap phase) and the difference is the largest at the end of out-stroke due to substantial deformation of the wing surface that lags behind the leading edge spar during a flap cycle.

It becomes clear that oscillatory behavior of the forces caused by the sub-flap inertial and aerodynamic effects results in variation of the pitch angle in the free flying DelFly thus also changing the effective angle of attack, as indicated in Figure 6(d). Although the test points for the free flight and wind tunnel measurements are not exactly the same in terms of angle of attack and forward flight speed, the X forces compare well for both cases with an approximately equal mean force generation (relative difference of 5%) over the flapping cycles (Figure 6(a)). There is a slight difference (relative difference of 12%) in the peak amplitudes, possibly due to aerodynamic damping effects in the free flight condition (Figure 6(c)). The small phase difference between the two cases, on the other hand, can be attributed to the discrete sampling time of the visual tracking system, resulting in a lag between the generation of the force and the observation of motion of 5ms, i.e., $1/200$Hz.

Forces in the body normal direction along the stroke plane (Z forces) were, however, considerably different both in terms of amplitude and phase of the force generation

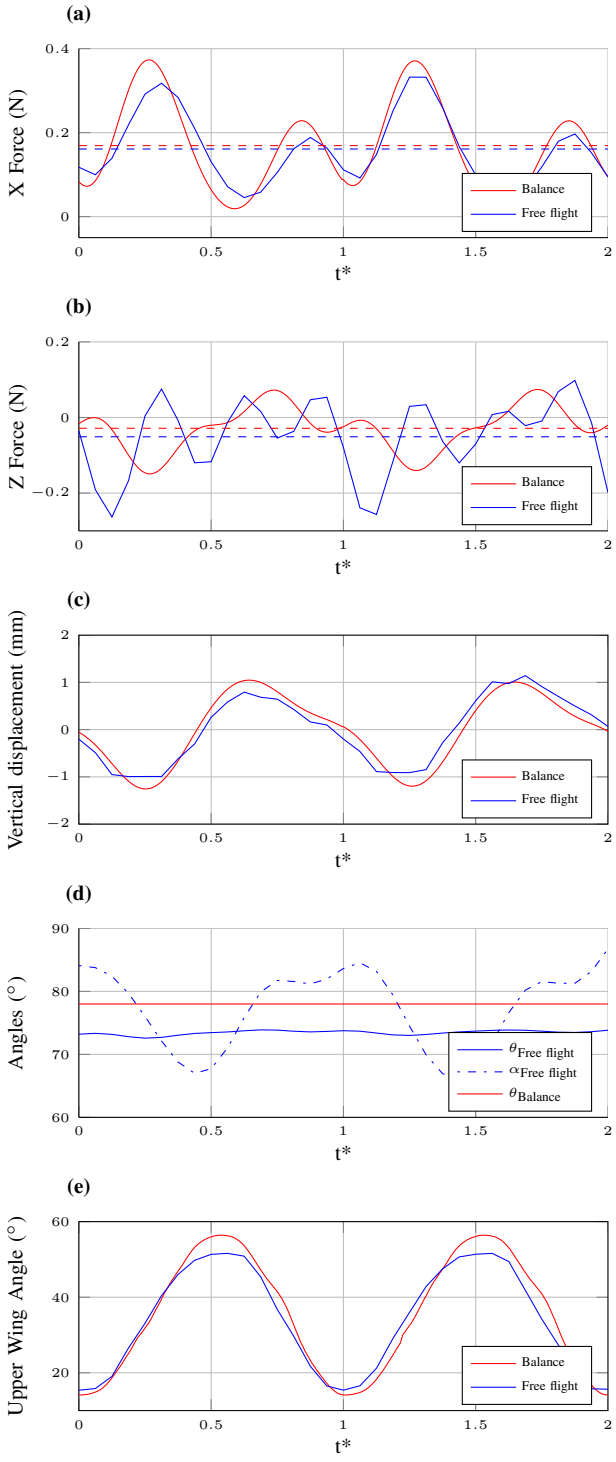

Fig. 6. (a) Longitudinal (X) and (b) normal force (Z) in the Body reference frame, (c) vertical displacement of the FWMAV, (d) pitch angles, and (e) upper wing's stroke angle in tethered (balance) and free flight condition for two flapping periods.

(Figure 6(b)). Two reasons were found: first, the clamping of the ornithopter in the wind tunnel balance measurements has a negative effect in the measurement of the Z forces, which can be even more affected with improper clamping positions. A simulation in CATIA showed that when clamped the first two structural dynamic modes of the DelFly body (which is a hollow carbon rod with a square cross section of 2mm×2mm), are excited inducing vibrations and displacements in vertical and lateral directions, i.e., in pitch and yaw, which contaminate the Z force, and thus barely affecting the X force;

Second, the different contributions of the tail in both free flight and tethered conditions also affect the force generation in the Z direction. As indicated in Figure 6(d), the angle of attack of the DelFly changes continuously during the free flight flapping cycle which in turn induces different flow conditions around the tail, when compared to non-pitching wind tunnel measurements. Moreover, the tethered nature of the wind tunnel experiments seems to neglect the pitch induced oscillatory tail contributions. Hence, it is expected that the force balance would predominately measure the forces that are induced by the flapping wings (both aerodynamic and inertial).

These results not only suggest that the tail effects that are captured in free flight are not detected in rigid tethered condition, but also show that wind tunnel tests can lead to wrong conclusions about the force generation mechanisms of a FWMAV.

Lift and Thrust forces are the most common force framework in the aeronautical community as these forces represent the longitudinal acting forces over an aerial vehicle having a direct relevance in the flight performance. Hence, Lift and Thrust were computed from X and Z, with Lift being the force perpendicular to the free-stream and Thrust the force along the free stream vector. The results are presented in Figure 7.

As indicated in Figure 7, the Lift and Thrust are considerably different across both experimental techniques. This is mainly due to the difference in the Z force, depicted in Figure 6(b). The average of the Lift (in a dashed line) is similar to for both methods, which indicates an approximate flap cycle average force, which is enough to counteract weight vector contribution. The average of Thrust, on the other hand, is very close to zero as this is a trimmed flight condition. Wind tunnel measurements show a small positive thrust due to non-matching dynamics the measurements in terms of tail contribution and clamping effects.

These results highlight the effects of tethered wind tunnel experimental techniques on the comprehension of flapping wing force characterization. In particular, it is shown that tethered wind tunnel force measurement techniques are only suitable for the characterization of the forces acting over the full FWMAV along the axis that is perpendicular to the stroke plane; it is also shown that the measurement of forces along the stroke plane can be contaminated by the structural dynamic modes, given the low mass and low stiffness of FWMAV structures.

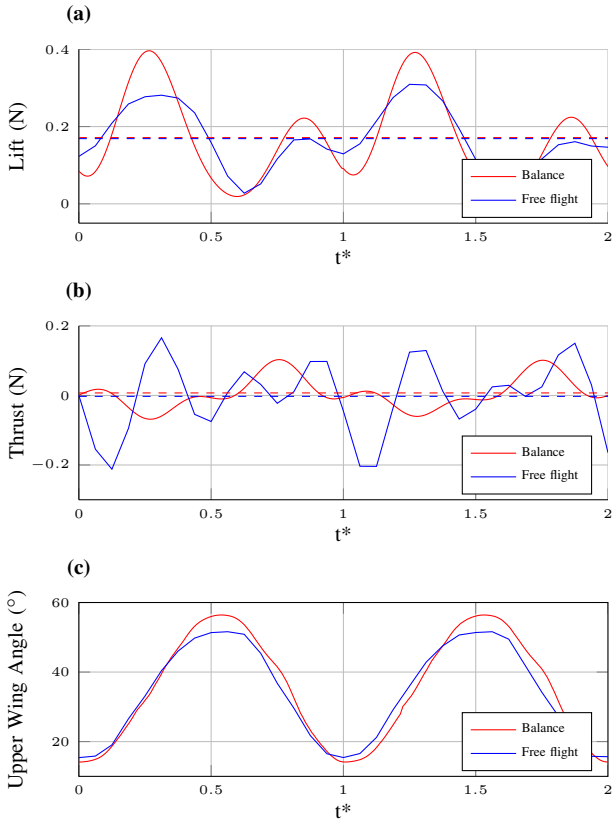

Fig. 7. (a) Lift, (b) Thrust and (c) upper wing stroke angle in tethered (force balance) and free flight conditions for two flapping periods. The wind tunnel results (red) fail to compare with the free flight (blue), mainly due to the different Z force identified in both experimental methods. The average force is indicated with a dashed line, with respective color.

IV. Concluding Remarks

Subflap longitudinal forces acting on a FWMAV were measured using a six axis force transducer in tethered wind tunnel and also calculated from free flight information captured by an external visual tracking system. Results were repeatable through a multitude of test flight regimes ranging from 0.3m/s to 2m/s and are shown for a trimmed flight condition with free stream velocity of 0.5 m/s, a pitch angle of 78°and a flapping frequency of 12.5Hz, for two flap cycles.

The longitudinal force along the Body reference frame (X) was found to be very similar for the two measurement methods. The amplitude differences were concluded to come from the dampening effects of air in the free flight case, when compared to the rigidly attached tests in the wind tunnel; a 5ms phase lag is due to the visual tracking system sampling frequency, equivalent to 1/200Hz.

The body normal force (Z), on the other hand, shows a considerable difference between both methods, due to absence of the rocking oscillatory motion (roll, pitch and yaw moment generation associated with the CG displacement) in the tethered wind tunnel measurements and thus different contributions of the tail and the air dampening effects. Furthermore, the dynamic structural modes of the ornithopter's body have a considerable effect on the body normal forces which appear when it is clamped on the force sensor,

corrupting the stroke plane force measurements, which can lead to bad force identification and characterization.

These results clearly showed that both methods yield very similar force measurement in the direction perpendicular to the stroke plane (X force). However, fixed wind tunnel force measurements lack on important dynamics of the FWMAV that are present in free flight and add negative effects of structural dynamics due to clamping of the fuselage, resulting in erroneous body normal force measurements and, ultimately, incorrect Lift and Thrust characterization. Thus, proper dynamic terms and contributions should be taken into account, i.e., the influence of the clamping mechanism and its position should be carefully studied and cross-compared with other experimental or simulation methods when assessing the flapping forces from fixed wind tunnel experimental tests.

REFERENCES

[1] C. Ellington, "The aerodynamics of hovering insect flight. i. the quasi-steady analysis," *Philosophical Transactions of the Royal Society of London. B, Biological Sciences*, vol. 305, no. 1122, pp. 1–15, 1984.

[2] C. Ellington, C. Berg, A. van den Willmott, and A. Thomas, "Leading-edge vortices in insect flight," *Nature*, vol. 384, no. 19/26, pp. 626–630, 1996.

[3] C. P. Ellington, "The novel aerodynamics of insect flight: Applications to micro-air vehicles," *Journal of Experimental Biology*, vol. 202, pp. 3439–3448, 1999.

[4] M. H. Dickinson and S. P. S. F. O. Lehmann, "Wing rotation and the aerodynamic basis of insect flight," *Science*, vol. 284, pp. 1954–1960, 1999.

[5] Z. J. Wang, "Two dimensional mechanism for insect hovering," *Physical Review Letters*, vol. 85, pp. 2219–2219, 2000.

[6] Z. J. Wang, "Dissecting insect flight," *Annual Rev. Fluid Mechanics*, vol. 37, pp. 183–210, 2005.

[7] A. Gogulapati and P. Friedmann, "Approximate aerodynamic and aeroelastic modeling of flapping wings in hover and forward flight," in *AIAA Structures, Structural Dynamics and Materials Conference*, no. 2011-2008, (Denver, Colorado, USA), AIAA, April 2011.

[8] H. Aono, S. Chimakurthi, C. E. Cesnik, H. Liu, and W. Shyy, "Computational modeling of spanwise flexibility effects on flapping wing," in *47th AIAA Aerospace Sciences Meeting*, AIAA, 2009.

[9] C. Kang, H. Aono, and C. E. Cesnik, "Effects of flexibility on the aerodynamic performance of flapping wings," in *6th AIAA Theoretical Fluid Mechanics Conference*, no. 2011-3121, (Hawaii), AIAA, June 2011.

[10] S. A. Ansari, K. Knowles, and R. Zbikowski, "Insectlike flapping wings in the hover part 1: Effect of wing kinematics," *Journal of Aircraft*, vol. 45, pp. 1945–1954, November 2008.

[11] S. A. Ansari, K. Knowles, and R. Zbikowski, "Insectlike flapping wings in the hover part 2: Effect of wing geometry," *Journal of Aircraft*, vol. 45, pp. 1976–1990, November 2008.

[12] M. A. Bolender, "Rigid multi-body equations-of-motion for flapping wing MAVs using Kane equations," in *AIAA Guidance, Navigation, and Control Conference*, no. 2009-6158, AIAA, August 2009.

[13] C. T. Orlowski, A. R. Girard, and W. Shyy, "Derivation and simulation of the nonlinear dynamics of a flapping wing micro-air vehicle," EMAV Sept 14-17, 2009.

[14] C. T. Orlowski and A. R. Girard, "Modeling and simulation of nonlinear dynamics of flapping wing micro air vehicles," *AIAA Journal*, vol. 49, no. 5, pp. 969–981, 2011.

[15] K. Sibilski, "Dynamics of micro-air-vehicle with flapping wings," *Acta Polytechna*, vol. 44, no. 2, pp. 15–21, 2004.

[16] K. Sibilski, J. Pietrucha, and M. Zlocka, "The comparative evaluation of power requirements for fixed, rotary, and flapping wings micro air vehicles," in *AIAA Atmospheric Flight Mechanics Conference and Exhibit*, no. 2007-6498, (Hilton Head, South Carolina), AIAA, August 2007.

[17] J. M. Dietl and E. Garcia, "Stability in ornithopter longitudinal flight dynamics," *Journal of Guidance, Control and Dynamics*, vol. 31, pp. 1157–1162, 2008.

[18] J. M. Dietl, T. Herrmann, G. Reich, and E. Garcia, "Dynamic modeling, testing, and stability analysis of an ornithoptic blimp," *Journal of Bionic Engineering*, vol. 8, no. 8, pp. 375–386, 2011.

[19] R. Wood, "The first takeoff of a biologically-inspired at-scale robotic insect," *IEEE Tranactions on Robotics*, vol. 24(2), pp. 341–347, 2008.

[20] P. Chirarattananon, K. Y. Ma, and R. J. Wood, "Adaptive control for takeoff, hovering, and landing of a robotic fly," in *Proceedings IEEE/RSJ International Conference on Intelligent Robots and Systems*, (Tokyo, Japan), pp. 3808–3815, November 2013.

[21] R. Fearing, K. Chiang, M. Dickinson, D. Pick, M. Sitti, , and J. Yan, "Wing transmission for a micromechanical flying insect," in *Proceedings of IEEE International Conference on Robotics & Automation*, (San Francisco), pp. 1509–1516, IEEE, April 2000.

[22] S. Baek and R. Fearing, "Flight forces and altitude regulation of 12 gram i-bird," in *IEEE RAS and EMBS International Conference on Biomedical Robotics and Biomechatronics (BioRob)*, pp. 454–460, 2010.

[23] J. Grauer and J. H. Jr., "Modeling of ornithopter flight dynamics for state estimation and control," AIAA, July 2010.

[24] J. Grauer, E. Ulrich, J. H. Jr., D. Pines, , and J. S. Humbert, "Testing and system identification of an ornithopter in longitudinal flight," *Journal of Aircraft*, vol. 48, pp. 660–667, March-April 2011.

[25] J.-S. Lee and J.-H. Han, "Experimental study on the flight dynamics of a bioinspired ornithopter: free flight testing and wind tunnel testing," *Journal of Smart Materials and Structures*, vol. 21, 2012.

[26] C. Lin and S. H. nd W. B. Young, "The thrust and lift of an ornithopters membrane wings with simple flapping motion," *Aerospace Science and Technology*, vol. 10, pp. 111–119, October 2005.

[27] A. Muniappan, V. Baskarand, and V. Duriyanandhan, "Lift and thrust characteristics of flapping wing micro air vehicle (mav)," in *43rd AIAA Aerospace Sciences Meeting and Exhibit - Meeting Papers*, AIAA, January 2005.

[28] K. Mazaheri and A. Ebrahimi, "Experimental investigation on aerodynamic performance of a flapping wing vehicle in forward flight," *Journal of Fluids and Structures*, vol. 27, pp. 586–595, April 2011.

[29] T. Nakata, H. Liu, Y. Tanaka, N. Nishihashi, X. Wang, and A. Sato, "Aerodynamics of a bio-inspired flexible flapping-wing micro air vehicle," *Bioinspiration & Biomimetics*, vol. 6, 2011.

[30] G. Lim, S. Shkarayev, Z. Goff, and P. Beran, "Studies of flight kinematics of ornithopters," in *International Competition and Conference on Micro Air Vehicles, IMAV 2012*, IMAV 2012, 2012.

[31] J. V. Caetano, C. C. de Visser, B. Remes, C. de Wagter, and M. Mulder, "Modeling a Flapping Wing MAV: Flight Path Reconstruction of the DelFly II," in *AIAA Modeling and Simulation Technologies*, AIAA, 2013.

[32] J. V. Caetano, C. de Visser, G. de Croon, B. Remes, C. de Wagter, J. Verboom, and M. Mulder, "Linear aerodynamic model identification of a flappingwing mav based on flight test data," *International Journal of Micro Air Vehicles*, vol. 5, pp. 273–286, December 2013.

[33] J. V. Caetano, C. C. de Visser, B. Remes, C. de Wagter, and M. Mulder, "Controlled flight maneuvers of a flapping wing micro air vehicle: a step towards the DelFly II identification," in *AIAA Atmospheric Flight Mechanics Conference*, 2013.

[34] Delfly Team, "Delfly." www.delfly.nl, accessed on January 5th, 2014.

[35] J. M. Dietl and E. Garcia, "Stability in hovering ornithopter flight," vol. 6930, SPIE Industrial and Commercial Applications of Smart Structures Technologies, 2008.

[36] J. M. Dietl and E. Garcia, "Ornithopter optimal trajectory control," *Aerospace Science and Technology*, vol. 26, p. 192199, AprilMay 2013.

[37] M. Percin, H. Eisma, B. van Oudheusden, B. Remes, R. Ruijsink, and C. de Wagter, "Flow Visualization in the Wake of the Flapping-Wing MAV 'DelFly II' in Forward Flight," in *AIAA Applied Aerodynamics Conference*, AIAA, 2012.

[38] T. Atherton and D. Kerbyson, "Size invariant circle detection," *Image and Vision Computing*, vol. 17, no. 11, pp. 795 – 803, 1999.

[39] M. Percin, H. Eisma, B. van Oudheusden, B. Remes, R. Rujsink, and C. de Wagter, "Flow visualization in the wake of flapping-wing MAV 'DelFly II' in forward flight," in *AIAA Fluid Dynamics and Co-located Conferences and Exhibit New Orleans*, 2012.